



# 1 A multi-decadal climatology of dust-on-snow from wet deposition in 2 the Upper Colorado River Basin

3 Felix W. Yu<sup>1,2</sup>, Daniel R. Feldman<sup>1</sup>, Leah D. Gibson<sup>1</sup>, William J. Rudisill<sup>1</sup>

4 <sup>1</sup>Earth and Environmental Sciences Area, Lawrence Berkeley National Laboratory, Berkeley, 94720, United States

5 <sup>2</sup>Energy and Resources Group, University of California, Berkeley, Berkeley, 94720, United States

6 *Correspondence to:* Felix W. Yu ([feyu@berkeley.edu](mailto:feyu@berkeley.edu)), Daniel R. Feldman ([drfeldman@lbl.gov](mailto:drfeldman@lbl.gov))

7 **Abstract.** Dust-on-snow deposition is the dominant factor in earlier snowmelt timing in the Upper Colorado River Basin  
8 (UCRB), which gets ~70% of its annual streamflow from snowmelt. Previous studies have demonstrated the radiative effects  
9 of dust-on-snow deposition, but have not quantified what deposition types, whether from atmospheric turbulence (dry  
10 deposition) or hydrometeor scavenging (wet deposition), drive these radiative effects. Here, we produce a climatology of the  
11 total amount and type of dust-on-snow deposition in the UCRB using the Modern-Era Retrospective analysis for Research  
12 and Applications (MERRA-2) reanalysis dataset from 1980-2023 and evaluate its accuracy using Surface Atmosphere  
13 Integrated Laboratory (SAIL) field measurements taken in 2022 and 2023 and Moderate Resolution Imaging Spectrometer  
14 (MODIS) Snow Property Inversion from Remote Sensing (SPIReS) dust concentration data. The results show that wet  
15 deposition is the dominant form of dust-on-snow deposition in the UCRB, comprising 73.8% of total dust deposition.  
16 Additionally, the eastern areas in the UCRB, particularly the Gunnison Watershed, experience 16% higher wet deposition  
17 monthly totals (69.33 mg m<sup>-2</sup>) than the entire UCRB average (59.80 mg m<sup>-2</sup>). These results highlight the importance of  
18 persistent spatial patterns but also interannual variability in accounting for dust deposition. This climatology also  
19 contextualizes the long-term records of dust deposition by showing how the relationships between dust at several sites with  
20 decadal records project onto the entire Basin, while also supporting water resource planning, especially for areas with  
21 elevated wet deposition levels.

## 22 1 Introduction

23 The Colorado River is one of the most important rivers in the US, providing water resources for 40 million people and  
24 helping to power 4.2 gigawatts of hydroelectric capacity (U.S. Bureau of Reclamation, 2012). The Upper Colorado River  
25 Basin (UCRB), which stretches across 5 Western states, provides nearly 90% of the Colorado River's total flow (McCabe  
26 and Wolock, 2007). However, the UCRB has faced drought conditions for over 20 years, which has stressed its water  
27 resources (McCabe et al., 2024). Within mountainous areas like the UCRB, snowmelt accounts for 70% of the total runoff  
28 and is vital to sustaining the Western water supply (Li et al., 2017). The dominant control on snowmelt timing in the UCRB  
29 is the deposition of mineral dust on snow, with dust comprising 90% of the concentration of light absorbing particles in the



30 area (Skiles and Painter, 2017). Mineral dust is composed of soil particles with diameters ranging from 0.1 - 50  $\mu\text{m}$ , although  
31 dust particles larger than 6  $\mu\text{m}$  have limited transport (Ginoux et al., 2001) and most deposited dust is transported from  
32 hundreds to tens of thousands of kilometers away (Painter et al., 2010; Neff et al., 2008; Heald et al., 2006; Chin et al., 2007;  
33 Wells et al., 2007). Dust particles in the snow decrease the snow's albedo, leading to increased radiative forcing (RF) that  
34 accelerates snowmelt by 3-7 weeks compared to a clean snowpack (Naple et al., 2025). Rapid snowmelt due to dust  
35 deposition decreases total runoff due to increased evapotranspiration and produces errors in snowmelt forecasting, straining  
36 water resources in an already drought-stressed area (Painter et al., 2010). Therefore, a robust understanding of the UCRB's  
37 water resources necessitates a characterization of the spatiotemporal dynamics of dust-on-snow deposition.

38

39 Dust deposition on snow can occur through two main ways: wet deposition, where precipitation scavenges dust particles, and  
40 dry deposition, when dust settles through turbulent mixing and gravity without precipitation. Both types of deposition occur  
41 in the UCRB, with the majority of events appearing in the spring (Colorado Dust on Snow Program). Dust deposition events,  
42 especially wet deposition events, are difficult to quantify from a remote sensing perspective due to storm cloud cover  
43 obscuring sensor views and precipitation particle sizes dwarfing mineral dust particle sizes by a magnitude of 1000x  
44 (Adibiyi et al., 2023).

45

46 In-situ monitoring of UCRB dust deposition is the primary source of information on dust-on-snow events in the Basin but is  
47 limited to in-person observations of the number of deposition events and qualitative observations of the severity of each  
48 storm (Colorado Dust on Snow Program). Due to the remote sensing challenges and lack of quantitative in-situ data, we  
49 draw insights from a modeled dust deposition product from NASA's Modern-Era Retrospective Analysis for Research and  
50 Applications, Version 2 (MERRA-2).

51

52 Although some studies exist looking at dust-on-snow radiative forcing impacts and its effects on melt-out dates, runoff, and  
53 streamflow timing across the UCRB (Skiles and Painter et al., 2012, Deems et al., 2013, Bryant et al., 2013, Fassnacht et al.,  
54 2022, Naple et al., 2025), they do not quantify the amount of dust deposition at a basin-wide scale or investigate the  
55 differences between wet deposition and dry deposition. Studies outside of the UCRB have used the GEOS-Chem model to  
56 quantify total black carbon deposition and light absorbing particle impacts in the Tibetan Plateau (He et al., 2014, Hao et al.,  
57 2023). Others have used MERRA-2 in combination with WRF-Chem to quantify wet and dry deposition in the Sierra  
58 Nevada (Huang et al., 2022). MERRA-2 has also been used to study dust sources and transport in the Colorado Plateau  
59 (Huang et al., 2026). Thus, the goals for this study were to develop a dust-on-snow climatology that is differentiated by  
60 deposition type and explore how well the spatiotemporal patterns of dust deposition are known with the following questions:

- 61 1. How accurate is MERRA-2 at detecting dust-on-snow events, particularly with wet deposition?
- 62 2. What are the most significant climatological features of dust-on-snow in the UCRB?



63 3. How did the dust-on-snow deposition patterns recorded at the Surface Atmosphere Integrated Laboratory (SAIL)  
64 field campaign compare to the rest of the UCRB?

65

66 To examine the amount of dust-on-snow deposition across space and time in the UCRB, we use a MERRA-2 product over a  
67 long period of record (1980-2023) to develop a climatological analysis. We then compare the MERRA-2 product to the  
68 SAIL campaign measurements in Gothic, CO from 2022 - 2023 to validate the accuracy of the modeled product and  
69 contextualize in-situ observations temporally and spatially across the UCRB. Within the UCRB, we focus our analysis in the  
70 Gunnison Watershed, which provides 16% of natural streamflow to the UCRB (Miller et al., 2013) and contains the SAIL  
71 field site. We finally validate the MERRA-2 product using Moderate Resolution Imaging Spectrometer (MODIS) Snow  
72 Property Inversion from Remote Sensing (SPIReS) to analyze the measured dust concentration in the snow from a remote  
73 sensing perspective (Bair et al., 2021).

## 74 **2 Data and Methods**

75 Dust deposition totals were taken from the MERRA-2 Aerosol Diagnostics product (M2T1NXADG), which is an hourly  
76 two-dimensional reanalysis product that separates the deposition of different types of aerosols, from black carbon to mineral  
77 dust (GMAO & Pawson 2015). All dust deposition analysis used DUWT and DUDP quantities, which were M2T1NXADG  
78 variables representing rates of mineral dust wet deposition and mineral dust dry deposition, respectively. Dust deposition is  
79 split into 5 mass bins based on particle sizes, ranging from a radius size of 0.73 - 8  $\mu\text{m}$  (GMAO 2023). For our purposes, we  
80 summed up all dust deposition bins together to get a single deposition number, as our analysis concerns all sizes of dust  
81 deposition. The resolution of the MERRA-2 product is 0.625 x 0.5 degrees (longitude x latitude) which translates to a ~54km  
82 x ~55km resolution in meters across the UCRB.

83

84 The MERRA-2 model simulates dust entrainment, transport, evolution, and deposition using the Goddard Chemistry Aerosol  
85 Radiation and Transport (GOCART) model coupled with the Goddard Earth Observing System (GEOS) (Ginoux et al.,  
86 2001). This dust is transported by advection along with turbulent and convective mixing and then is removed through  
87 simulated dry deposition (Wesely 1989) and wet deposition (Liu et al., 2001, Wang et al., 2011). Wet deposition removal is  
88 based on MERRA-2 precipitation fluxes and typical scavenging efficiencies of liquid and solid precipitation (Colarco et al.,  
89 2014, Randles et al., 2016). Because MERRA-2 is a reanalysis dataset, data lags real-time measurements by a few weeks to  
90 account for assimilation using historical precipitation and aerosol measurements.

91

92 In-situ data on dust deposition dates and types were obtained from the SAIL Campaign conducted in Gothic, CO from 2021-  
93 2023 (Feldman et al., 2023). Dust deposition events were identified by detecting increased aerosol concentrations through an  
94 Optical Particle Counter (OPC) and decreases in 415 nm surface albedo from a SKYRAD broadband instrument (Gibson et



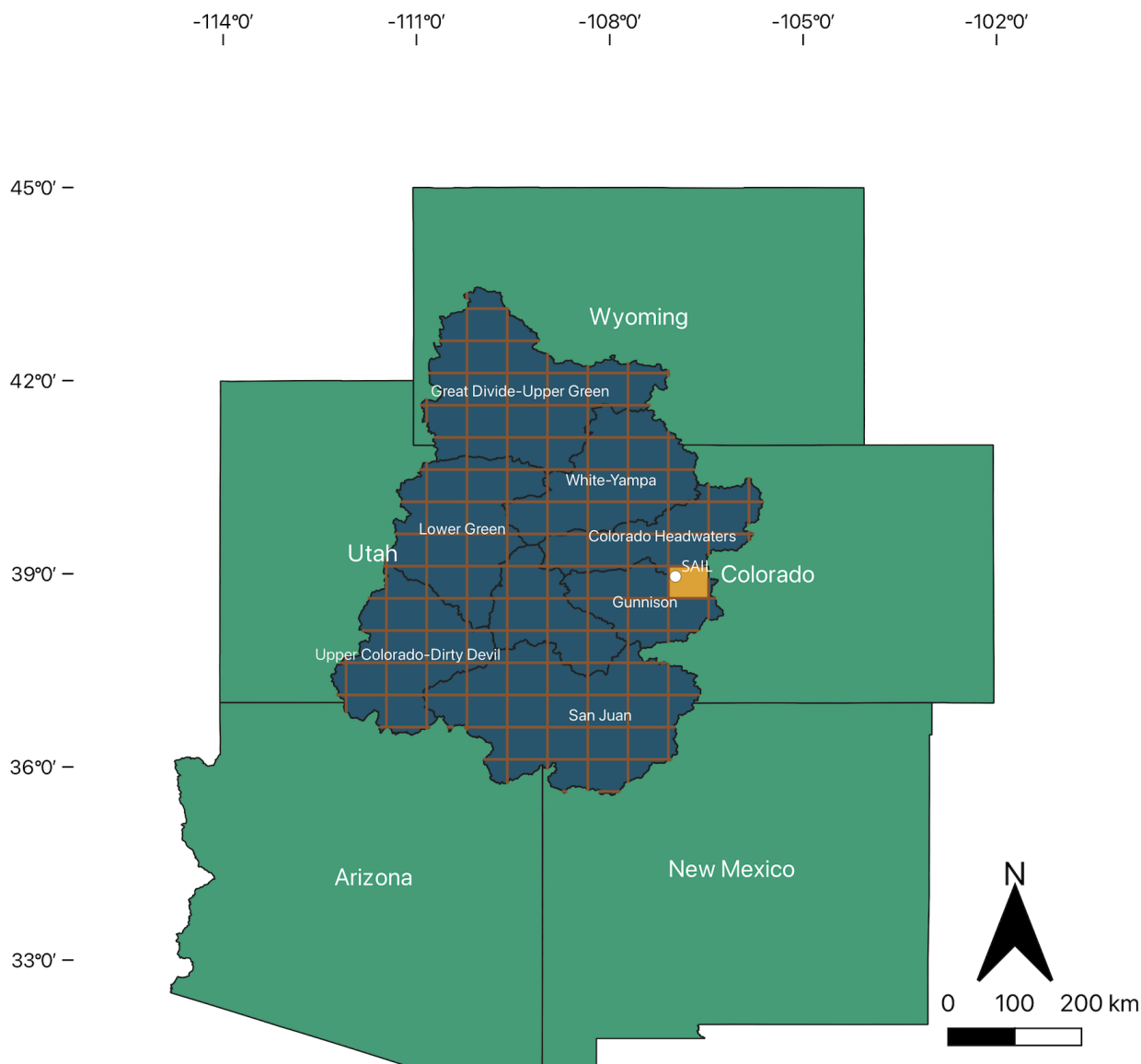
95 al., 2025). Wet deposition events were characterized by increases in precipitation data from a Pluvio2-L weighing bucket  
96 (Zhu et al., 2021) and lagged surface albedo changes. Dry deposition events had no precipitation bucket events and  
97 immediate surface albedo effects (Gibson et al., 2025).

98

99 To compare dust deposition to the presence of dust in the snow on the ground, we took dust concentration data in parts per  
100 million weight (ppmw) from a remotely sensed MODIS SPIReS 500m product (Bair et al., 2021). This product estimates the  
101 dust concentration in a snow-covered pixel by computing the scattering properties of light-absorbing particles (LAPs) using  
102 the Mie theory. Then, it uses a spectral mixing linear mixture model to solve for multiple variables, including dust  
103 concentration, snow-covered area, photometric shade, and grain radius, by minimizing the modeled surface reflectance and  
104 observed surface reflectance from MOD09GA. Therefore, additional dust deposition on the snowpack would theoretically  
105 lead to higher dust concentration values for the snowpack. Although SPIReS cannot differentiate between the concentrations  
106 of different LAPs (such as black carbon versus dust), this is of limited concern in the UCRB context, as the dominant LAP  
107 during spring melt is mineral dust (Naple et al., 2025), and black carbon's effect on snow albedo is spectrally  
108 indistinguishable from that of dust from a MODIS standpoint (Bair et al., 2021). This algorithm performs similarly in  
109 accuracy for estimating snow albedo compared to MODIS Snow Covered Area and Grain-size (MODSCAG) and MODIS  
110 Dust Radiative Forcing in Snow (MODDRFS), but has the advantage of directly obtaining dust concentrations instead of  
111 additional radiative forcing due to dust (Painter et al., 2009, Painter et al., 2012, Palomaki et al., 2025).

112

113 All outputs were clipped to the UCRB shapefile taken from the United States Geological Survey's (USGS) Watershed  
114 Boundary Dataset 2-digit hydrologic unit, and the Gunnison Watershed in this study refers to the USGS 4-digit hydrologic  
115 unit within the UCRB.



116

117 **Figure 1: Map of the Upper Colorado River Basin in MERRA-2 grid resolution**

118 **2.1 Validation of MERRA-2 Data with SAIL Data**

119 SAIL field data shows 17 total dust-on-snow deposition events from February 2022 - April 2023 with 13 wet deposition  
120 events and 4 dry deposition events (Table 1). We pulled MERRA-2 DUWT (Dust Wet Deposition) and DUDP (Dust Dry  
121 Deposition) data from the same time period (February 2022 - April 2023) at a pixel over the SAIL site near Gothic, CO at  
122 38.96° N, 106.99° W. Although the resolution of this data (~55km) is larger than area represented by field measurements,  
123 previous analysis shows there is minimal variability in aerosol concentrations on at daily timescales across the East River



124 Watershed, and therefore these two data products can be compared (Gibson et al., 2025). Hourly MERRA-2 data was then  
125 summed to a single daily total. We created a histogram of each year's monthly dust deposition data split into 6 different dust  
126 deposition bins categorized by the amount of dust deposition in  $\mu\text{g m}^{-2}$ , with each day's dust deposition as an input. Wet  
127 deposition was histogrammed separately from dry deposition. The bins were thresholded such that a majority of days with no  
128 dust deposition fell into the first bin, while the second bin onwards captured days of dust deposition. These dust deposition  
129 days were then compared to the SAIL field data. The number of bins for each month was adjusted to capture the number of  
130 SAIL dust deposition days as closely as possible.

## 131 **2.2 Comparison with MERRA-2 Climatology**

132 To contextualize the 2022-2023 UCRB MERRA-2 dust deposition results to the historical dust deposition mean, we develop  
133 a climatology of the MERRA-2 dataset from 1980 - 2023 for both dry deposition and wet deposition for the months of  
134 February, March, April, and May (the heaviest recorded months for dust-on-snow deposition). We summed the total  
135 cumulative dry and wet deposition separately for each month and year and then took the average across all years in the  
136 period to develop a 43-year climatological mean for each month for both wet and dry deposition. This corresponds to the  
137 length of the MERRA-2 record, which itself is driven by the introduction of modern satellite technology, especially with the  
138 Television and InfraRed Observation Satellite - N (TIROS-N) systems. We also calculate the standard deviation for each  
139 month across the 43-year period to measure interannual variability. The percentage of wet versus dry deposition was  
140 calculated by adding together wet and dry deposition to get total dust deposition, then dividing each component by the total  
141 dust deposition amount.

142

143 We also summed the total dry and wet deposition from MERRA-2 for the pre-melt snow water year (November - May) for  
144 2022 and 2023. This total accumulates all the winter and spring precipitation and dust deposition that affects snowmelt. All  
145 summed pixels in a region were spatially averaged together to get one dust deposition value for each region.

146

147 To see if additional precipitation was the only factor for increased wet deposition, we calculated a Spearman's rank  
148 correlation coefficient ( $\rho$ ) between total MERRA-2 precipitation and total wet deposition for 2022 and 2023 in the UCRB.  
149 Spearman's correlation coefficient is a non-parametric measure of correlation between two variables without assumptions of  
150 the underlying distribution of each variable (Spearman 1904). Like an  $r^2$  value,  $\rho$  ranges from -1 to 1, indicating the strength  
151 of correlation.

152

153 Finally, to assess the anomalousness of wet deposition during the SAIL campaign years (2022 and 2023), we computed z-  
154 scores using the climatological mean and standard deviation as the population parameters. The z-score method has been used  
155 in previous studies to compare MERRA-2 dust aerosols and dust deposition across multiple time periods (Zamora et al.,  
156 2022, Bolaño-Ortiz et al., 2023) and is widely used in drought analysis to detect precipitation anomalies (Wu et al., 2002,



157 Ford 2014). Each campaign year's wet deposition total was treated as a sample observation, allowing us to express its  
158 departure from the long-term climatological average in the context of an outlier analysis. Z-scores were calculated for each  
159 area of the analysis within the UCRB separately, ensuring that the same area was compared across different years. We  
160 converted the monthly climatology means to a single aggregated climatology mean, and the 2022 and 2023 monthly sample  
161 means to two yearly aggregated sample means using Eq. (1), where  $N_i$  is the number of days in each month and  $\mu_i$  is each  
162 month's wet deposition mean.

$$163 \mu = \frac{\sum_i^n N_i \mu_i}{\sum_i^n} \quad (1)$$

164 By using the law of total variance, we translated the monthly standard deviations into a combined single standard deviation  
165 using Eq. (2), where  $Var(X)$  is the total variance across time or space,  $Var(X|i)$  is the variance for each pixel or month's wet  
166 deposition,  $\mu_i$  is taken from Eq. (1), and  $\sigma_i$  is each pixel or each month's wet deposition standard deviation.

$$167 Var(X) = E[Var(X|i)] + Var(E[X|i])$$

$$168 Var(X) = E[\sigma_i^2] + Var(\mu_i) \quad (2)$$

$$169 \sigma = \sqrt{Var(X)}$$

170 Finally, we used the means and standard deviations to calculate a z-score for the 2022 and 2023 wet deposition totals using  
171 Eq. (3), where  $\mu_s$  is the 2022 or 2023 wet deposition mean calculated from Eq. (1),  $\mu_c$  is the 43-year climatology mean  
172 calculated from Eq. (1), and  $\sigma_c$  is the 43-year climatology standard deviation calculated from Eq. (2).

$$173 z = \frac{\mu_s - \mu_c}{\sigma_c} \quad (3)$$

### 174 2.3 SPIReS Dust Concentration Analysis

175 Historical SPIReS scenes from February - June of 2022 and 2023 were downloaded from the National Snow and Ice Data  
176 Center. Because MODIS scenes have a different projection based on a tiling system, we downloaded three different tiles that  
177 together cover the UCRB: h09v04, h09v05, and h10v04. The three tiles were mosaiced together using rioarray's  
178 "merge\_arrays" method, then reprojected using nearest neighbor to EPSG:4326 using rioarray's "reproject" method.  
179 Because dust deposition on snow builds up over successive events and accumulates over time before fully emerging as the  
180 snowpack melts, we took the maximum dust concentration value across the melt season (February-June) for each pixel to  
181 account for this accumulation phenomenon. Previous work has linked SPIReS dust concentration as a proxy of clean  
182 snowpack and used the date of maximum MODDRFS, a similar product, as a representation of maximum dust accumulation  
183 on the snowpack (Bair et al., 2021, Naple et al., 2025). All 500m maximum pixels in a region were spatially averaged  
184 together to get one SPIReS dust concentration value for each region, including the Gunnison Watershed and the wider  
185 UCRB.

186



187 After resampling the 500m maximum SPIReS aggregation to 55km using the average resampling method, we masked out  
188 any pixels with less than 25% valid SPIReS pixels for both the SPIReS dataset and corresponding MERRA-2 pixel. Invalid  
189 SPIReS pixels exist where the SPIReS fractional snow cover never reaches above or equal to 0.10 (Bair et al., 2021). We  
190 calculated a Spearman’s correlation coefficient to measure the correlation between dust deposition and the snowpack’s dust  
191 concentration. We then compared the SPIReS changes for 2022 and 2023 for each area in the basin against the changes in  
192 total MERRA-2 dust deposition to assess whether MERRA-2 dust deposition amounts aligned directionally with observed  
193 dust concentration levels.

### 194 3. Results

195 Wet deposition was the dominant type of dust deposition in the UCRB. Wet deposition accounted for 73.8% of MERRA-2’s  
196 total dust deposition, and dry deposition contributed 26.2% to total dust deposition from 1980 - 2023. This is consistent with  
197 the SAIL field data, where 13/17 (76%) were wet deposition events and 4/17 (24%) were dry deposition events (Table 1).  
198 Wet deposition events were easier to identify than dry deposition events using MERRA-2, as the magnitude of the total dust  
199 deposition was significantly elevated (>8x the normal average) during wet deposition events (Figures 1&2) compared to dry  
200 deposition events (<1.5x the normal average). Due to the elevated effect of wet deposition events in the UCRB, the increased  
201 ability of MERRA-2 to detect these events, and the difficulty of wet deposition detection by traditional remote sensing  
202 methods, we decided to focus our MERRA-2 validation analysis with SAIL data on wet deposition.

(a) WY2022 Deposition Date	Deposition Type	Detected by MERRA-2
February 22, 2022	Wet	Yes
March 5, 2022	Wet	Yes
March 31, 2022	Wet	No
April 12, 2022	Wet	Yes
April 20, 2022	Dry	N/A*
April 22, 2022	Wet	No

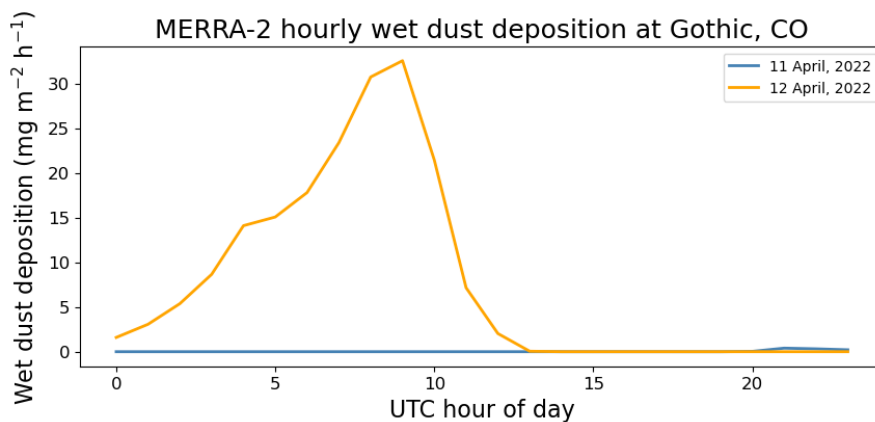


May 2, 2022	Wet	Yes
May 3, 2022	Wet	No
May 8, 2022	Dry	N/A*
May 9, 2022	Dry	N/A*

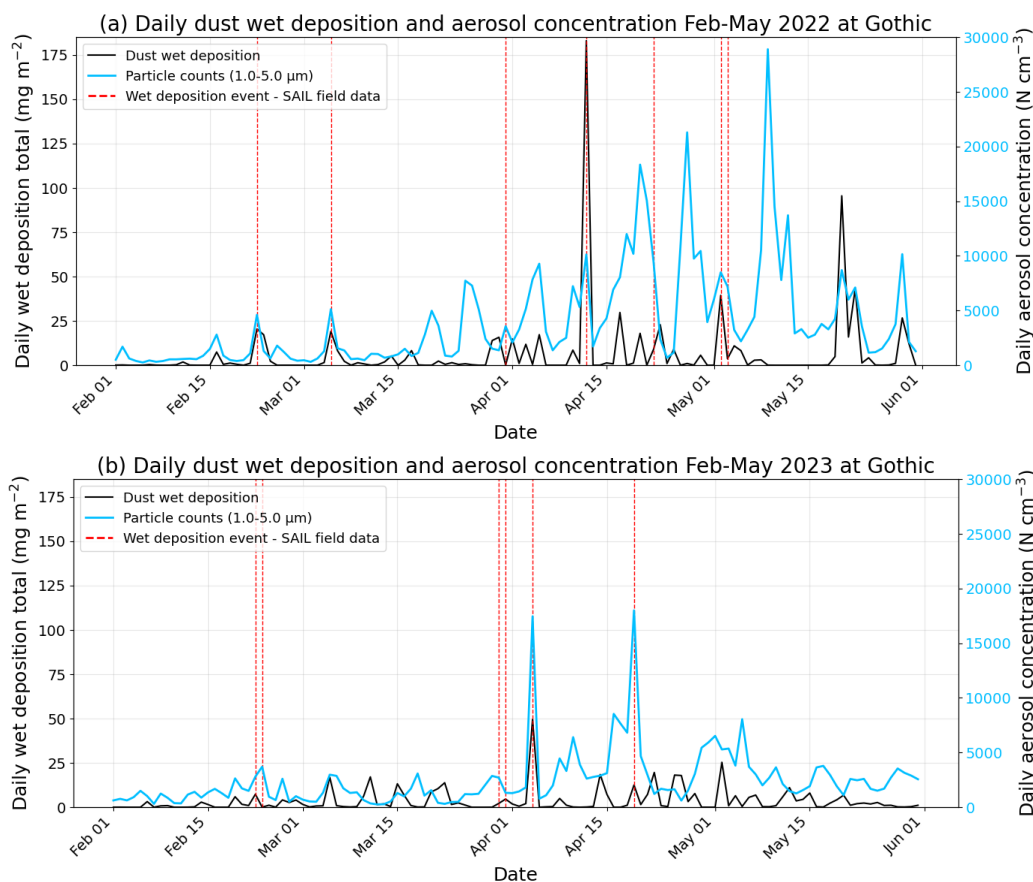
203

<b>(b) WY2023 Deposition Date</b>	<b>Deposition Type</b>	<b>Detected by MERRA-2</b>
February 22, 2023	Wet	Yes
February 23, 2023	Wet	No
March 5, 2023	Dry	N/A*
March 30, 2023	Wet	No
March 31, 2023	Wet	Yes
April 4, 2023	Wet	Yes
April 19, 2023	Wet	Yes

204 **Table 1: Dates and type of dust deposition events identified at SAIL, along with MERRA-2 threshold detection agreement for 2022**  
205 **(a) and 2023 (b). \*Individual dry deposition events were not analysed with MERRA-2.**



206 **Figure 2: Hourly view of the largest daily deposition event at the SAIL site on 12 April 2022 compared to a normal deposition day**  
207 **on 11 April 2022**



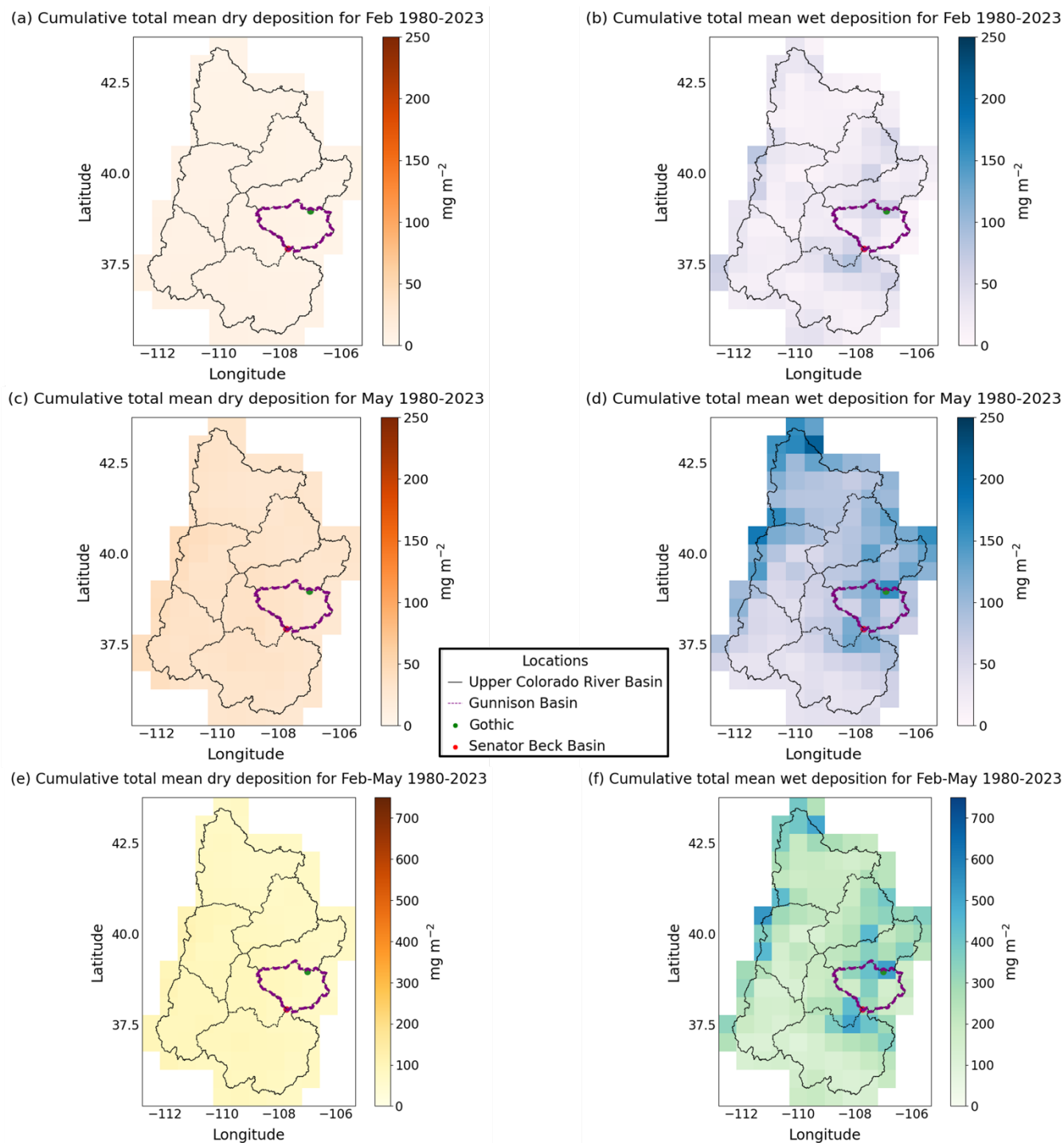
208 **Figure 3: MERRA-2 daily wet deposition totals ( $\text{mg m}^{-2}$ ) for 2022 (a) and 2023 (b) over the SAIL site location in Gothic, CO.**



209 **3.1 MERRA-2 Validation and Climatology Results**

210 MERRA-2 was able to detect most wet deposition events that occurred at SAIL, identifying 8/13 (62%) wet deposition  
211 events successfully (Table 1). These wet deposition events (Figure 2) were accompanied by higher supermicron aerosol  
212 concentrations observed in the field, which are indicative of dust in the area (Figure 3). Both dry deposition and wet  
213 deposition amounts were lowest in February and higher in May, tracking the higher aerosol concentrations observed during  
214 the later spring months (Figure 4). Additionally, dry deposition was more uniformly distributed throughout the UCRB  
215 compared to wet deposition, which had a heterogeneous spatial pattern (Figure 4).

216

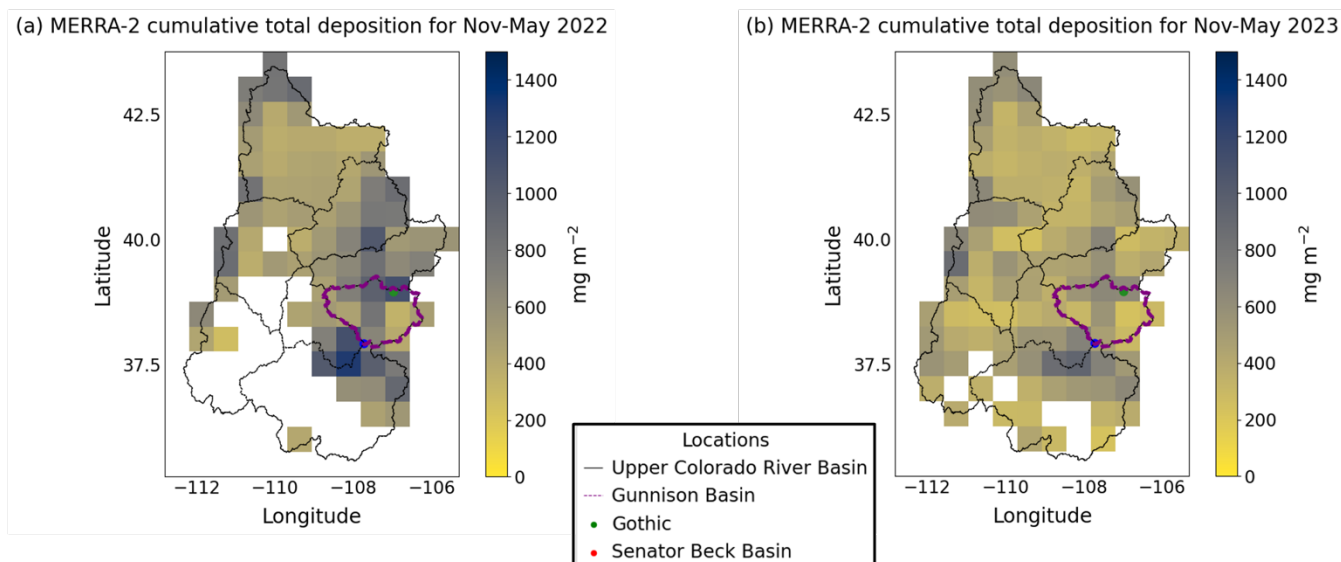


217  
218  
219

Figure 4: UCRB outline of MERRA-2 dust deposition data. (a) and (c) show dry deposition and (b) and (d) show wet deposition for individual climatology months. (e) and (f) show total average dry and wet deposition for the total 4-month deposition period



220 The Gunnison Watershed experienced 16% higher monthly dust wet deposition averages for the MERRA-2 climatology  
 221 dataset from February - May ( $69.33 \text{ mg m}^{-2}$ ) compared to the whole UCRB region ( $59.80 \text{ mg m}^{-2}$ , Figure 4). In particular,  
 222 the mean monthly wet deposition value over the SAIL site was 114% higher ( $127.79 \text{ mg m}^{-2}$ ) than the UCRB average.



223  
 224 **Figure 5: UCRB Outline of total dry and wet deposition from the WY 2022 (a) and WY 2023 (b) spanning November 2021 - May**  
 225 **2022 and November 2022 - May 2023. Pixels with less than 25% of snow cover are masked out**

226

Water Year	UCRB Total Deposition ( $\text{mg m}^{-2}$ )	UCRB Average Deposition ( $\text{mg m}^{-2}$ )	Gunnison Watershed Mean Deposition ( $\text{mg m}^{-2}$ )	SAIL Site Mean Deposition ( $\text{mg m}^{-2}$ )	SAIL Site vs. UCRB Average % Difference	Gunnison Watershed vs UCRB % Difference
2022	48077	608.58	685.63	1110.22	+82%	+13%
2023	46119	452.15	464.96	638.99	+41%	+3%
% Yearly Change	-4%	-4%	-32%	-42%	-41%	-10%

227 **Table 2: Summary of changes in total dust deposition in the UCRB region in WY2022 and WY2023 taken from Figure 5**

228 The SAIL site experiences significantly more total dust deposition (82% in 2022 and 41% in 2023) than the UCRB, while  
 229 the Gunnison Watershed experienced slightly more total dust deposition than the UCRB in 2022 (+13%) and 2023 (+3%).



230 The entire UCRB experienced more dust deposition in 2022 than 2023. The Spearman’s coefficient calculation between  
231 MERRA-2’s wet deposition and corrected precipitation variables yield a value of 0.42 with a p-value below 0.001.

232 **3.2 Z-score Results**

Location	2022 Z-score	2023 Z-Score
UCRB	0.24	0.08
Gunnison Watershed	0.50	-0.02
SAIL Site (Gothic, CO)	0.80	-0.22

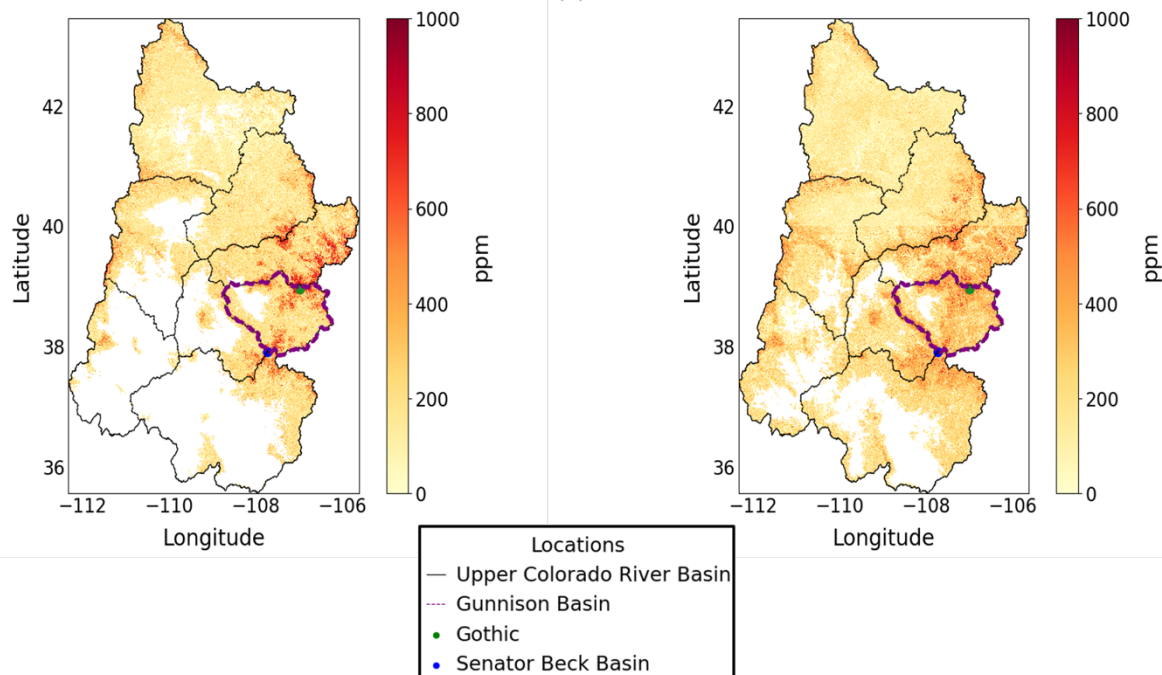
233 **Table 3: Z-scores comparing the total average monthly wet deposition from February - May in 2022/2023 to the 43-year February**  
234 **- May climatological total average monthly wet deposition in the same area**

235 During the 2022–2023 SAIL campaign years, UCRB z-scores indicate slightly above-average wet deposition compared to  
236 the climatology average, with 2022 dustier than 2023 (Table 3). This pattern is reflected in the field data, with one additional  
237 wet deposition event recorded in 2022 compared to 2023 (Table 1). In 2023, although wet deposition was elevated across the  
238 UCRB, the Gunnison Watershed and SAIL site recorded below-average deposition relative to climatology. None of the years  
239 showed an extreme deviance of wet deposition compared to the climatological average, as all z-score magnitudes were less  
240 than 1.0.

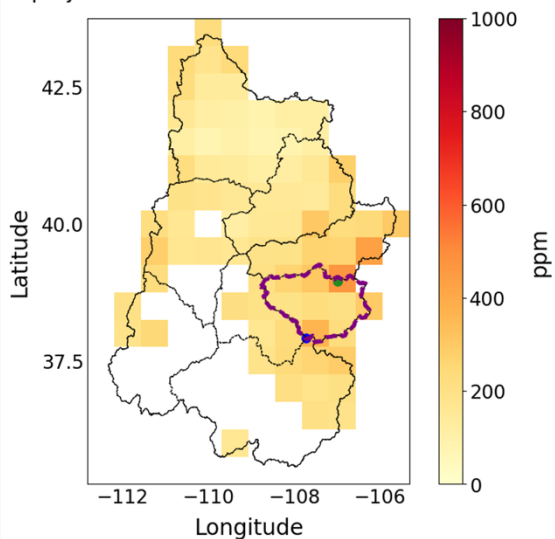


241 **3.3 SPIReS Result**

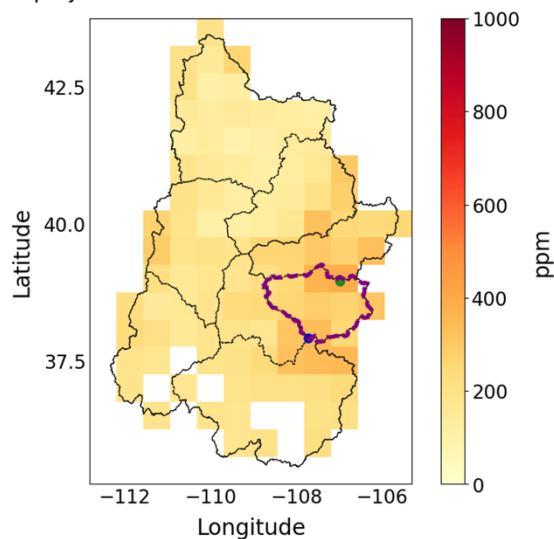
(a) Max SPIReS dust concentration at 500m resolution for 2022 (b) Max SPIReS dust concentration at 500m resolution for 2023



(c) Max SPIReS dust concentration projected to MERRA-2 resolution for 2022



(d) Max SPIReS dust concentration projected to MERRA-2 resolution for 2023



242

243 **Figure 6: UCRB outline of MODDRFS data. (a) and (b) show SPIReS dust concentration data at the original 500m resolution for**  
244 **February - June (the melt season) 2022 vs 2023. (c) and (d) show SPIReS dust concentration values resampled to MERRA-2 55km**  
245 **resolution in 2022 vs 2023**

246



<b>Water Year</b>	<b>Average UCRB SPIReS (ppm)</b>	<b>Average Gunnison Watershed SPIReS (ppm)</b>	<b>SAIL Site SPIReS (ppm)</b>	<b>SAIL Site vs. UCRB % Difference</b>	<b>Gunnison Watershed vs. UCRB % Difference</b>
2022	195.18	270.84	503.0	+158%	+39%
2023	199.39	299.44	453.0	+127%	+50%
Yearly % Change	+2%	+11%	-10%	-31%	+11%

247 **Table 4: Max 500m SPIReS values averaged across all pixels in a respective region for February - June of each year.**

248 The spearman correlation coefficient between total MERRA-2 dust deposition from WY 2022 and WY 2023 and maximum  
 249 SPIReS dust concentration during the 2022 and 2023 melt season was 0.63 and 0.44 with p-values below 0.001, respectively.  
 250 The SPIReS data over the UCRB showed similar trends spatially to MERRA-2, with a higher dust concentration in both the  
 251 Gunnison and SAIL site when compared to the broader UCRB (+39% and +158%). The SAIL site showed a decrease in dust  
 252 concentration from 2022 to 2023, consistent with MERRA-2's modelled decrease in total dust deposition over the same  
 253 period. However, the SPIReS dataset showed a slight increase in dust concentration for the UCRB and the Gunnison Basin  
 254 from 2022 to 2023, whereas MERRA-2 showed a slight decrease in dust deposition over the same regions from 2022 to  
 255 2023.

256 **4. Discussion**

257 **4.1 MERRA-2 and SPIReS Detection Accuracy and Limitations**

258 Although MERRA-2 was able to accurately detect the occurrence of most wet deposition events (62%) when validated with  
 259 field data in a particular location, the accuracy of the exact projected amounts of dust deposition is still unknown due to the  
 260 lack of quantitative field data in the area. The excess dust deposition days identified by MERRA-2 relative to the SAIL field  
 261 record are likely attributable to a combination of MERRA-2's coarse pixel resolution, which integrates deposition signals  
 262 from a broader area than the field site alone, and its known tendency to overestimate dust deposition flux over the Northern  
 263 Hemisphere (Koke et al., 2023). Accuracy could be further improved with the development of a finer-resolution dust



264 deposition model. Lastly, MERRA-2 does not distinguish between precipitation types of rain or snow in wet deposition,  
265 which may overestimate dust-on-snow in areas with low snowpack.

266

267 SPIReS has some known limitations when estimating dust concentration. In particular, the dust concentration is fixed at a  
268 measured peak value during melt out, and an optically thick layer of snow is assumed during calculation. Thus, the  
269 maximum dust concentration may be an underestimate of the total amount of dust in the snow, as dust layers usually  
270 aggregate together during spring snowmelt (Naple et al., 2025). Additionally, the main goal for the SPIReS dust  
271 concentration estimation is to mimic the LAP's effect on snow albedo instead of maximizing the accuracy of the total  
272 amount of dust concentration in the snow (Bair et al., 2021). Therefore, the actual amount of dust concentration in the snow  
273 may differ compared to the numbers reported by SPIReS. Lastly, remote sensing retrievals have uncertainties due to cloud  
274 cover and must make assumptions about snow grain and dust particle sizes. Even with these limitations, we still believe that  
275 SPIReS is a valuable tool to inspect the larger temporal and spatial observational patterns of dust concentrations in the  
276 snowpack.

277

278 When comparing MERRA-2 with SPIReS, we see that MERRA-2 and SPIReS generally align on dust-in-snow spatially and  
279 have a slight disagreement temporally. There is a clear spatial correlation between MERRA-2 dust deposition and observed  
280 SPIReS dust concentration, as seen through the spearman's correlation coefficient between MERRA-2 and SPIReS (0.63 in  
281 2022 and 0.44 in 2023). Both MERRA-2 and SPIReS data agree that the SAIL site and the Gunnison Watershed experience  
282 higher amounts of dust deposition and dust concentration than the UCRB, with less deposition and concentration at the SAIL  
283 site from 2022 to 2023. MERRA-2 and SPIReS disagree slightly regarding dust deposition versus dust concentration at the  
284 UCRB and Gunnison Watershed from 2022 to 2023. MERRA-2 shows a slight decrease in dust deposition versus SPIReS'  
285 slight increase in dust concentration from 2022 to 2023. Because the magnitude of temporal differences is small, whether the  
286 disagreement is due to MERRA-2 errors, SPIReS errors, spatial upscaling of SPIReS to MERRA-2 resolution, or a  
287 disconnect between dust deposition and dust concentration remains to be seen. Lastly, we note that comparing dust  
288 deposition fluxes to observed snowpack dust concentrations represents a simplification of snow-dust interaction dynamics.  
289 While the limited spatial coverage and availability of in-situ dust deposition measurements preclude direct quantitative  
290 validation of MERRA-2, the correlated patterns between modeled dust deposition and observed snowpack dust  
291 concentrations provide support for the MERRA-2's reliability in simulating dust deposition in this region.

#### 292 **4.2 SAIL Field Campaign Comparisons to the Larger UCRB**

293 In general, the MERRA-2 climatology shows that the Gunnison Watershed receives more dust deposition on average than  
294 the rest of the UCRB. Because dry dust deposition is largely spatially uniform, areas like the Gunnison with heavier wet  
295 deposition experience higher total dust deposition. Within the Gunnison Watershed, the SAIL region receives more dust  
296 deposition than average. Specifically, 2022 was a higher dust deposition year than average for SAIL (0.80 z-score), and 2023



297 was closer to an average dust deposition year (-0.22 z-score). Thus, during the field campaign, 2023 is a more representative  
298 year for total dust deposition than 2022. This contrasts with total snowfall for each year, where 2022 was close to the median  
299 snow-water equivalent for the Gunnison Watershed and 2023 was a higher-than-normal snow-water equivalent year (NRCS  
300 2022 & 2023). Additionally, a Spearman's coefficient of 0.42 between precipitation and wet deposition demonstrates that  
301 while increased precipitation is correlated with increased wet deposition, precipitation alone cannot capture the patterns of  
302 wet deposition.

### 303 **4.3 Applications to dust monitoring and other models**

304 Currently, important work is being done by the Colorado Dust on Snow Program (CODOS) to track dust deposition event  
305 types and dates, along with qualitative observations of dust on the snowpack, for water resource management. With a more  
306 sophisticated dust deposition detection algorithm validated with known CODOS dust deposition dates, the MERRA-2  
307 dataset could be utilized to understand dust deposition types and events in areas where in-person observations are scarce, too  
308 difficult to obtain, or obscured due to weather. Additional field measurements of direct dust-on-snow deposition quantities  
309 would provide a means to validate the accuracy of the model's simulated deposition rates beyond event detection accuracy,  
310 unlocking the full potential of dust deposition analyses. Future work will connect MERRA-2 deposition rates to some  
311 existing measured black carbon and mineral dust concentrations (Gleason et al. 2022).

312

313 Operational snow and water supply forecasting models, such as iSnobal, SNOW17, or M<sup>4</sup> are vital to understand and predict  
314 the timing and magnitude of snowmelt runoff (Marks et al., 1999, Anderson 2006; Fleming et al, 2021). However, known  
315 model gaps exist, particularly due to the exclusion of dust deposition events that change the albedo of the snow within these  
316 models (Meyer et al., 2023). Incorporating MERRA-2 dust deposition data with remote sensing solutions into these models  
317 could improve predictions and fill in gaps, particularly during hard to detect wet deposition events.

### 318 **5. Conclusion**

319 The impact of light-absorbing particles, especially dust, on snowpack dynamics, can hardly be overstated in the mountain  
320 west (Painter et al, 2010; Skiles et al, 2018, Fassnacht et al, 2022). Yet the physical processes by which dust deposits onto  
321 the snowpack, remain complex and very difficult to observe (Lawrence and Neff, 2009). Direct estimates of dust deposition  
322 itself beyond just the exposure of dust radiative impacts of snow are important to pinpoint the timing, type, and total amounts  
323 of dust deposition in different areas in the UCRB, especially since dust deposition can impact snowmelt and water resources  
324 (Painter et al., 2010). However, wet deposition processes, even though they are central to dust deposition dynamics in the  
325 UCRB, are particularly difficult to measure because the clouds and precipitation that are co-occurring with dust wet  
326 deposition necessarily interfere with optical remote sensing in the wavelengths typically used for dust remote sensing.



327 Therefore, assimilation approaches are a useful way to understand the processes and total amount of dust deposition, which  
328 are missing in existing literature over the UCRB area.

329

330 This study quantified dust deposition patterns across the Upper Colorado River Basin from 1970-2023 with a focus on the  
331 Gunnison Watershed and the SAIL field campaign site in Gothic, CO. Our findings show that MERRA-2 can be used to  
332 understand spatial and temporal trends in dust deposition in the UCRB, as MERRA-2 detected a majority (62%) of wet  
333 deposition events over the Gothic, CO area when compared to field data from 2022-2023. Within the UCRB, wet deposition  
334 is the dominant form of dust deposition, comprising ~74% of total dust deposition in the area and exhibiting more spatial  
335 heterogeneity than dry deposition.

336

337 Spatial climatological trends show eastern areas of the UCRB receive more wet deposition than average, with the Gunnison  
338 Watershed receiving 16% more monthly wet deposition ( $69.33 \text{ mg m}^{-2}$ ) than the UCRB average ( $59.80 \text{ mg m}^{-2}$ ) from 1970-  
339 2023. During the years of the SAIL field campaign, the SAIL site received significantly more total dust-on-snow deposition  
340 compared to the UCRB in 2022 (82%) and in 2023 (41%). The SAIL site received slightly more total dust-on-snow  
341 deposition than the Gunnison Watershed in 2022 (13%) and in 2023 (3%). This means that the SAIL field data cannot  
342 accurately represent dust-on-snow deposition rates in the broader UCRB but are representative of dust-on-snow deposition in  
343 the Gunnison Watershed. Based on a z-score analysis, neither 2022 (0.80) nor 2023 (-0.22) total dust-on-snow deposition  
344 amounts at the SAIL site were significantly anomalous compared to the climatological record in the same area. Thus, the  
345 SAIL field campaign was a representative sample within the wider temporal context of dust-on-snow deposition in its  
346 associated area.

347

348 It should be noted that MERRA-2 potentially overestimates total dust deposition in the UCRB, as it detects more wet  
349 deposition events over the SAIL site than were recorded. Whether this over detection stems from MERRA-2's coarse spatial  
350 resolution including other deposition events in the area or its inherent detection accuracy remains an open question that  
351 additional field data on dust deposition amounts across the region could help resolve. This overestimation tendency is  
352 consistent with previous studies of MERRA-2 dust concentration simulations in other areas (Buchard et al., 2017).

353

354 Datasets that are proven to be competent in dust deposition will be increasingly important as they will enable researchers to  
355 study not just pieces of dust impacts on snow, but the entire life cycle: from entrainment to transport to deposition to albedo  
356 impacts. This life cycle, while populated by processes that may at first appear to be straightforward to characterize, has many  
357 sizable gaps, and wet deposition is, arguably, the largest of those gaps. This process is exceedingly difficult to observe  
358 directly with remote sensing, as electromagnetic scattering from hydrometeors dominates the scattering from dust, and  
359 hydrometeor scattering changes imperceptibly with dust scavenging. Even with in-situ measurements, aerosol collects are  
360 swamped by hydrometeors, and even the signal of wet deposition in snow pits is subtle. However, we show here that



361 MERRA-2, by assimilating dust, transporting it, and including aerosol-precipitation scavenging, is indeed competent at  
362 capturing spatial and temporal patterns of dust deposition in the UCRB.

363

364 We can use this to develop a climatology and have done so here. This climatology reveals consistent, persistent patterns of  
365 deposition, and points to the dominance of wet deposition as the vehicle for dust deposition in the UCRB, especially in  
366 certain areas like the Gunnison Watershed.

367

368 These findings can support water resource prediction, especially where sub-seasonal timing and amount are critical. For  
369 those applications where the prediction of snow melt-out across the UCRB requires sub-weekly accuracy, we show that  
370 advancing aerosol-precipitation interaction science is necessary.

#### 371 **Data availability**

372 The Optical Particle Counter (OPC), Pluvio2-L weighing bucket, and SKYRAD data collected during the SAIL campaign  
373 are available on the ARM data discovery portal.

374 The MERRA-2 M2T1NXADG data is available through the NASA Earthdata Portal.

375 The historical SPIReS is available through the National Snow and Ice Data Center.

376 The Watershed Boundary Dataset is available through the United States Geological Survey.

377 Links to MERRA-2, SPIReS, OPC, and Pluvio2-L weighing bucket data are provided below.

378

379 MERRA-2 Climatology Dataset: <https://doi.org/10.5281/zenodo.19957854>

380 MERRA-2 M2T1NXADG: [https://disc.gsfc.nasa.gov/datasets/M2T1NXADG\\_5.12.4/summary](https://disc.gsfc.nasa.gov/datasets/M2T1NXADG_5.12.4/summary)

381 Historical SPIReS: [https://nsidc.org/data/spires\\_hist/versions/1](https://nsidc.org/data/spires_hist/versions/1)

382 Pluvio2-L Weighing Bucket:

383 [https://adc.arm.gov/discovery/#!/results/id::gucwbpluvio2M1.a1\\_accum\\_total\\_nrt\\_upperair\\_wb\\_sfcmet?dataLevel=a1&show](https://adc.arm.gov/discovery/#!/results/id::gucwbpluvio2M1.a1_accum_total_nrt_upperair_wb_sfcmet?dataLevel=a1&showDetails=true)  
384 [Details=true](https://adc.arm.gov/discovery/#!/results/id::gucwbpluvio2M1.a1_accum_total_nrt_upperair_wb_sfcmet?dataLevel=a1&showDetails=true)

385 Optical Particle Counter (OPC):

386 [https://adc.arm.gov/discovery/#!/results/id::gucaosopcS2.b1\\_dN\\_dlogDp\\_microchem\\_opc\\_aerosol?dataLevel=b1&showDeta](https://adc.arm.gov/discovery/#!/results/id::gucaosopcS2.b1_dN_dlogDp_microchem_opc_aerosol?dataLevel=b1&showDetails=true)  
387 [ils=true](https://adc.arm.gov/discovery/#!/results/id::gucaosopcS2.b1_dN_dlogDp_microchem_opc_aerosol?dataLevel=b1&showDetails=true)

388 Watershed Boundary Dataset:

389 <https://www.usgs.gov/national-hydrography/watershed-boundary-dataset>



390 **Author contributions**

391 D.R.F and F.Y. conceptualized the research. F.Y. carried out general analysis, visualization, validation, and first draft of the  
392 manuscript. D.R.F coordinated, funded, and guided the research. W.J.R. contributed to the SPIReS dust concentration  
393 analysis. L.D.G. analyzed dust deposition field data. All authors edited the manuscript.

394 **Competing interests**

395 The authors declare that they have no conflict of interest.

396 **Disclaimer**

397 “Copernicus Publications remains neutral with regard to jurisdictional claims made in the text, published maps, institutional  
398 affiliations, or any other geographical representation in this paper. While Copernicus Publications makes every effort to  
399 include appropriate place names, the final responsibility lies with the authors. Views expressed in the text are those of the  
400 authors and do not necessarily reflect the views of the publisher.”

401 **Acknowledgements**

402 This work used data and built upon analysis from the Atmospheric Radiation Measurement’s Surface Atmosphere Integrated  
403 Field Laboratory and National Aeronautics and Space Administration’s Global Modeling and Assimilation Office.

404 **Financial support**

405 This work was supported by the U.S. Department of Energy, Office of Science, Office of Biological and Environmental  
406 Research and the Atmospheric System Research Program under U.S. Department of Energy Contract No. DE-AC02-  
407 05CH11231. This work used resources of the National Energy Research Scientific Computing Center, a DOE Office of  
408 Science User Facility supported by the Office of Science of the U.S. Department of Energy, under that same contract.

409 **References**

410 Adebisi, A., Kok, J. F., Murray, B. J., Ryder, C. L., Stuu, J.-B. W., Kahn, R. A., Knippertz, P., Formenti, P., Mahowald, N.  
411 M., Pérez García-Pando, C., Klose, M., Ansmann, A., Samset, B. H., Ito, A., Balkanski, Y., Di Biagio, C., Romanias, M. N.,  
412 Huang, Y., and Meng, J.: A review of coarse mineral dust in the Earth system, *Aeolian Research*, 60, 100849,  
413 <https://doi.org/10.1016/j.aeolia.2022.100849>, 2023.

414



- 415 Anderson, E.: Snow Accumulation and Ablation Model – SNOW-17, last access: 22 April 2026.  
416
- 417 Bair, E. H., Stillinger, T., and Dozier, J.: Snow Property Inversion From Remote Sensing (SPIReS): A Generalized  
418 Multispectral Unmixing Approach With Examples From MODIS and Landsat 8 OLI, *IEEE Transactions on Geoscience and*  
419 *Remote Sensing*, 59, 7270–7284, <https://doi.org/10.1109/TGRS.2020.3040328>, 2021.  
420
- 421 Bair, E., Stillinger, T., Rittger, K., and Skiles, M.: COVID-19 lockdowns show reduced pollution on snow and ice in the  
422 Indus River Basin, *Proceedings of the National Academy of Sciences*, 118, e2101174118,  
423 <https://doi.org/10.1073/pnas.2101174118>, 2021.  
424
- 425 Bolaño-Ortiz, T. R., Díaz-Gutiérrez, V. L., Vélez-Pereira, A. M., Vergara-Vásquez, E. L., and Camargo-Caicedo, Y.: Snow  
426 Albedo Reduction in the Colombian Andes Mountains Due to 2000 to 2020 Saharan Dust Intrusions Events, *Water*, 15,  
427 <https://doi.org/10.3390/w15173150>, 2023.
- 428 Bryant, A. C., Painter, T. H., Deems, J. S., and Bender, S. M.: Impact of dust radiative forcing in snow on accuracy of  
429 operational runoff prediction in the Upper Colorado River Basin, *Geophysical Research Letters*, 40, 3945–3949,  
430 <https://doi.org/10.1002/grl.50773>, 2013.
- 431 Buchard, V., Randles, C. A., Silva, A. M. da, Darmenov, A., Colarco, P. R., Govindaraju, R., Ferrare, R., Hair, J.,  
432 Beyersdorf, A. J., Ziemba, L. D., and Yu, H.: The MERRA-2 Aerosol Reanalysis, 1980 Onward. Part II: Evaluation and  
433 Case Studies, <https://doi.org/10.1175/JCLI-D-16-0613.1>, 2017.
- 434 Bureau of Reclamation: Colorado River Basin Water Supply and Demand Study,  
435 <https://www.usbr.gov/lc/region/programs/crbstudy.html>, last access: 18 March 2026, 2012.
- 436 Chin, M., Diehl, T., Ginoux, P., and Malm, W.: Intercontinental transport of pollution and dust aerosols: implications for  
437 regional air quality, *Atmospheric Chemistry and Physics*, 7, 5501–5517, <https://doi.org/10.5194/acp-7-5501-2007>, 2007.
- 438 Colarco, P. R., Nowottnick, E. P., Randles, C. A., Yi, B., Yang, P., Kim, K.-M., Smith, J. A., and Bardeen, C. G.: Impact of  
439 radiatively interactive dust aerosols in the NASA GEOS-5 climate model: Sensitivity to dust particle shape and refractive  
440 index, *Journal of Geophysical Research: Atmospheres*, 119, 753–786, <https://doi.org/10.1002/2013JD020046>, 2014.
- 441 Colorado Dust-on-Snow Program: <http://www.codos.org>, last access: 18 March 2026.



- 442 Deems, J. S., Painter, T. H., Barsugli, J. J., Belnap, J., and Udall, B.: Combined impacts of current and future dust deposition  
443 and regional warming on Colorado River Basin snow dynamics and hydrology, *Hydrology and Earth System Sciences*, 17,  
444 4401–4413, <https://doi.org/10.5194/hess-17-4401-2013>, 2013.
- 445 Fassnacht, S. R., Duncan, C. R., Pfohl, A. K. D., Webb, R. W., Derry, J. E., Sanford, W. E., Reimanis, D. C., and Doskocil,  
446 L. G.: Drivers of Dust-Enhanced Snowpack Melt-Out and Streamflow Timing, *Hydrology*, 9,  
447 <https://doi.org/10.3390/hydrology9030047>, 2022.
- 448 Feldman, D. R., Aiken, A. C., Boos, W. R., Carroll, R. W. H., Chandrasekar, V., Collis, S., Creamean, J. M., Boer, G. de,  
449 Deems, J., DeMott, P. J., Fan, J., Flores, A. N., Gochis, D., Grover, M., Hill, T. C. J., Hodshire, A., Hulm, E., Hume, C. C.,  
450 Jackson, R., Junyent, F., Kennedy, A., Kumjian, M., Levin, E. J. T., Lundquist, J. D., O'Brien, J., Raleigh, M. S., Reithel, J.,  
451 Rhoades, A., Rittger, K., Rudisill, W., Sherman, Z., Siirila-Woodburn, E., Skiles, S. M., Smith, J. N., Sullivan, R. C.,  
452 Theisen, A., Tuftedal, M., Varble, A. C., Wiedlea, A., Wielandt, S., Williams, K., and Xu, Z.: The Surface Atmosphere  
453 Integrated Field Laboratory (SAIL) Campaign, <https://doi.org/10.1175/BAMS-D-22-0049.1>, 2023.
- 454 Fleming, S. W., Garen, D. C., Goodbody, A. G., McCarthy, C. S., and Landers, L. C.: Assessing the new Natural Resources  
455 Conservation Service water supply forecast model for the American West: A challenging test of explainable, automated,  
456 ensemble artificial intelligence, *Journal of Hydrology*, 602, 126782, <https://doi.org/10.1016/j.jhydrol.2021.126782>, 2021.
- 457 Ford, T. W.: Precipitation anomalies in Eastern-Central Iowa from 1640 – Present, *Journal of Hydrology*, 519, 918–924,  
458 <https://doi.org/10.1016/j.jhydrol.2014.08.021>, 2014.
- 459 Gelaro, R., McCarty, W., Suárez, M. J., Todling, R., Molod, A., Takacs, L., Randles, C. A., Darmenov, A., Bosilovich, M.  
460 G., Reichle, R., Wargan, K., Coy, L., Cullather, R., Draper, C., Akella, S., Buchard, V., Conaty, A., Silva, A. M. da, Gu, W.,  
461 Kim, G.-K., Koster, R., Lucchesi, R., Merkova, D., Nielsen, J. E., Partyka, G., Pawson, S., Putman, W., Rienecker, M.,  
462 Schubert, S. D., Sienkiewicz, M., and Zhao, B.: The Modern-Era Retrospective Analysis for Research and Applications,  
463 Version 2 (MERRA-2), <https://doi.org/10.1175/JCLI-D-16-0758.1>, 2017.
- 464 Gibson, L., Feldman, D., Aiken, A. C., Cowherd, M., and Riihimaki, L.: The Impact of Dust in Snowfall on Snow Albedo in  
465 the Upper Colorado River Basin, 105th AMS Annual Meeting, 2025.
- 466 Ginoux, P., Chin, M., Tegen, I., Prospero, J. M., Holben, B., Dubovik, O., and Lin, S.-J.: Sources and distributions of dust  
467 aerosols simulated with the GOCART model, *Journal of Geophysical Research: Atmospheres*, 106, 20255–20273,  
468 <https://doi.org/10.1029/2000JD000053>, 2001.



- 469 Gleason, K. E., McConnell, J. R., Arienzo, M. M., Sexstone, G. A., and Rahimi, S.: Black carbon dominated dust in recent  
470 radiative forcing on Rocky Mountain snowpacks, *Environ. Res. Lett.*, 17, 054045, <https://doi.org/10.1088/1748-9326/ac681b>, 2022.
- 472 Hao, D., Bisht, G., Rittger, K., Bair, E., He, C., Huang, H., Dang, C., Stillinger, T., Gu, Y., Wang, H., Qian, Y., and Leung,  
473 L. R.: Improving snow albedo modeling in the E3SM land model (version 2.0) and assessing its impacts on snow and surface  
474 fluxes over the Tibetan Plateau, *Geoscientific Model Development*, 16, 75–94, <https://doi.org/10.5194/gmd-16-75-2023>,  
475 2023.
- 476 He, C., Li, Q., Liou, K.-N., Takano, Y., Gu, Y., Qi, L., Mao, Y., and Leung, L. R.: Black carbon radiative forcing over the  
477 Tibetan Plateau, *Geophysical Research Letters*, 41, 7806–7813, <https://doi.org/10.1002/2014GL062191>, 2014.
- 478 Huang, H., Qian, Y., Liu, Y., He, C., Zheng, J., Zhang, Z., and Gkikas, A.: Where does the dust deposited over the Sierra  
479 Nevada snow come from?, *Atmospheric Chemistry and Physics*, 22, 15469–15488, <https://doi.org/10.5194/acp-22-15469-2022>, 2022.
- 481 Huang, H., Adebisi, A. A., Liu, Y., Chen, Z., Kibria, M., Wu, M., Qian, Y., and Wang, H.: Spring Dust in Colorado Plateau:  
482 Transport Pathways and Interannual Variability Derived From Two Decades of MERRA-2 Reanalysis, *Geophysical  
483 Research Letters*, 53, e2025GL119096, <https://doi.org/10.1029/2025GL119096>, 2026.
- 484 Heald, C. L., Jacob, D. J., Park, R. J., Alexander, B., Fairlie, T. D., Yantosca, R. M., and Chu, D. A.: Transpacific transport  
485 of Asian anthropogenic aerosols and its impact on surface air quality in the United States, *Journal of Geophysical Research:  
486 Atmospheres*, 111, <https://doi.org/10.1029/2005JD006847>, 2006.
- 487 Kok, J. F., Adebisi, A. A., Albani, S., Balkanski, Y., Checa-Garcia, R., Chin, M., Colarco, P. R., Hamilton, D. S., Huang, Y.,  
488 Ito, A., Klose, M., Leung, D. M., Li, L., Mahowald, N. M., Miller, R. L., Obiso, V., García-Pando, C. P., Rocha-Lima, A.,  
489 Wan, J. S., and Whicker, C. A.: Improved representation of the global dust cycle using observational constraints on dust  
490 properties and abundance, *Atmos Chem Phys*, 21, 8127–8167, <https://doi.org/10.5194/acp-21-8127-2021>, 2021.
- 491 Lawrence, C. R. and Neff, J. C.: The contemporary physical and chemical flux of aeolian dust: A synthesis of direct  
492 measurements of dust deposition, *Chemical Geology*, 267, 46–63, <https://doi.org/10.1016/j.chemgeo.2009.02.005>, 2009.
- 493 Li, D., Wrzesien, M. L., Durand, M., Adam, J., and Lettenmaier, D. P.: How much runoff originates as snow in the western  
494 United States, and how will that change in the future?, *Geophysical Research Letters*, 44, 6163–6172,  
495 <https://doi.org/10.1002/2017GL073551>, 2017.



- 496 Liu, H., Jacob, D. J., Bey, I., and Yantosca, R. M.: Constraints from  $^{210}\text{Pb}$  and  $^7\text{Be}$  on wet deposition and transport in a  
497 global three-dimensional chemical tracer model driven by assimilated meteorological fields, *Journal of Geophysical*  
498 *Research: Atmospheres*, 106, 12109–12128, <https://doi.org/10.1029/2000JD900839>, 2001.
- 499 Marks, D., Domingo, J., Susong, D., Link, T., and Garen, D.: A spatially distributed energy balance snowmelt model for  
500 application in mountain basins, *Hydrological Processes*, 13, 1935–1959, [https://doi.org/10.1002/\(SICI\)1099-](https://doi.org/10.1002/(SICI)1099-)  
501 [1085\(199909\)13:12/13%253C1935::AID-HYP868%253E3.0.CO;2-C](https://doi.org/10.1002/(SICI)1099-1085(199909)13:12/13%253C1935::AID-HYP868%253E3.0.CO;2-C), 1999.
- 502 McCabe, G. J. and Wolock, D. M.: Warming may create substantial water supply shortages in the Colorado River basin,  
503 *Geophysical Research Letters*, 34, <https://doi.org/10.1029/2007GL031764>, 2007.
- 504 McCabe, G. J. and Wolock, D. M.: Recent Declines in Western U.S. Snowpack in the Context of Twentieth-Century Climate  
505 Variability, <https://doi.org/10.1175/2009EI283.1>, 2009.
- 506 McCabe, G. J., Wolock, D. M., and Gangopadhyay, S.: Past and Projected Future Droughts in the Upper Colorado River  
507 Basin, *Geophysical Research Letters*, 51, e2023GL107978, <https://doi.org/10.1029/2023GL107978>, 2024.
- 508 Meyer, J., Horel, J., Kormos, P., Hedrick, A., Trujillo, E., and Skiles, S. M.: Operational water forecast ability of the HRRR-  
509 iSnoB combination: an evaluation to adapt into production environments, *Geoscientific Model Development*, 16, 233–250,  
510 <https://doi.org/10.5194/gmd-16-233-2023>, 2023.
- 511 Miller, W. P., DeRosa, G. M., Gangopadhyay, S., and Valdés, J. B.: Predicting regime shifts in flow of the Gunnison River  
512 under changing climate conditions, *Water Resources Research*, 49, 2966–2974, <https://doi.org/10.1002/wrcr.20215>, 2013.
- 513 Naple, P., Skiles, S. M., Lang, O. I., Rittger, K., Lenard, S. J. P., Burgess, A., and Painter, T. H.: Dust on Snow Radiative  
514 Forcing and Contribution to Melt in the Colorado River Basin, *Geophysical Research Letters*, 52, e2024GL112757,  
515 <https://doi.org/10.1029/2024GL112757>, 2025.
- 516 Neff, J. C., Ballantyne, A. P., Farmer, G. L., Mahowald, N. M., Conroy, J. L., Landry, C. C., Overpeck, J. T., Painter, T. H.,  
517 Lawrence, C. R., and Reynolds, R. L.: Increasing eolian dust deposition in the western United States linked to human  
518 activity, *Nature Geosci*, 1, 189–195, <https://doi.org/10.1038/ngco133>, 2008.
- 519 Painter, T. H., Bryant, A. C., and Skiles, S. M.: Radiative forcing by light absorbing impurities in snow from MODIS surface  
520 reflectance data, *Geophysical Research Letters*, 39, <https://doi.org/10.1029/2012GL052457>, 2012.



- 521 Painter, T. H., Deems, J. S., Belnap, J., Hamlet, A. F., Landry, C. C., and Udall, B.: Response of Colorado River runoff to  
522 dust radiative forcing in snow, *Proceedings of the National Academy of Sciences*, 107, 17125–17130,  
523 <https://doi.org/10.1073/pnas.0913139107>, 2010.
- 524 Painter, T. H., Rittger, K., McKenzie, C., Slaughter, P., Davis, R. E., and Dozier, J.: Retrieval of subpixel snow covered area,  
525 grain size, and albedo from MODIS, *Remote Sensing of Environment*, 113, 868–879,  
526 <https://doi.org/10.1016/j.rse.2009.01.001>, 2009.
- 527 Palomaki, R. T., Rittger, K., Lenard, S. J. P., Bair, E., Dozier, J., Skiles, S. M., and Painter, T. H.: Assessment of methods  
528 for mapping snow albedo from MODIS, *Remote Sensing of Environment*, 326, 114742,  
529 <https://doi.org/10.1016/j.rse.2025.114742>, 2025.
- 530 Randles, C. A., Pan, X., Smirnov, A., Yu, H., and Govindaraju, R.: The MERRA-2 Aerosol Assimilation, 45, n.d.
- 531 Skiles, S. M., Flanner, M., Cook, J. M., Dumont, M., and Painter, T. H.: Radiative forcing by light-absorbing particles in  
532 snow, *Nature Clim Change*, 8, 964–971, <https://doi.org/10.1038/s41558-018-0296-5>, 2018.
- 533 Skiles, S. M. and Painter, T.: Daily evolution in dust and black carbon content, snow grain size, and snow albedo during  
534 snowmelt, Rocky Mountains, Colorado, *Journal of Glaciology*, 63, 118–132, <https://doi.org/10.1017/jog.2016.125>, 2017.
- 535 Spearman, C.: The Proof and Measurement of Association between Two Things, *The American Journal of Psychology*, 15,  
536 72–101, <https://doi.org/10.2307/1412159>, 1904.  
537
- 538 Wang, Q., Jacob, D. J., Fisher, J. A., Mao, J., Leibensperger, E. M., Carouge, C. C., Le Sager, P., Kondo, Y., Jimenez, J. L.,  
539 Cubison, M. J., and Doherty, S. J.: Sources of carbonaceous aerosols and deposited black carbon in the Arctic in winter-  
540 spring: implications for radiative forcing, *Atmospheric Chemistry and Physics*, 11, 12453–12473,  
541 <https://doi.org/10.5194/acp-11-12453-2011>, 2011.
- 542 Wells, K. C., Witek, M., Flatau, P., Kreidenweis, S. M., and Westphal, D. L.: An analysis of seasonal surface dust aerosol  
543 concentrations in the western US (2001–2004): Observations and model predictions, *Atmospheric Environment*, 41, 6585–  
544 6597, <https://doi.org/10.1016/j.atmosenv.2007.04.034>, 2007.
- 545 Wesely, M. L.: Parameterization of surface resistances to gaseous dry deposition in regional-scale numerical models,  
546 *Atmospheric Environment* (1967), 23, 1293–1304, [https://doi.org/10.1016/0004-6981\(89\)90153-4](https://doi.org/10.1016/0004-6981(89)90153-4), 1989.
- 547 Wu, H., Hayes, M. J., Weiss, A., and Hu, Q.: An evaluation of the Standardized Precipitation Index, the China-Z Index and  
548 the statistical Z-Score, *International Journal of Climatology*, 21, 745–758, <https://doi.org/10.1002/joc.658>, 2001.



549 Zamora, L. M., Kahn, R. A., Evangeliou, N., Groot Zwaaftink, C. D., and Huebert, K. B.: Comparisons between the  
550 distributions of dust and combustion aerosols in MERRA-2, FLEXPART, and CALIPSO and implications for deposition  
551 freezing over wintertime Siberia, *Atmospheric Chemistry and Physics*, 22, 12269–12285, [https://doi.org/10.5194/acp-22-](https://doi.org/10.5194/acp-22-12269-2022)  
552 [12269-2022](https://doi.org/10.5194/acp-22-12269-2022), 2022.

### 553 **Dataset references**

554 Cromwell, E., Singh, A., and Kuang, C.: Optical Particle Counter (AOSOPC), 2021-10-27 to 2023-06-16, ARM Mobile  
555 Facility (GUC), Gunnison, CO; Supplemental Facility 2 (S2), Atmospheric Radiation Measurement (ARM) User Facility  
556 [data set], <https://doi.org/10.5439/1824224>, 2021.

557

558 Global Modeling and Assimilation Office (GMAO): MERRA-2 tavg1\_2d\_adg\_Nx: 2d,1-Hourly,Time-Averaged,Single-  
559 Level,Assimilation,Aerosol Diagnostics (Extended) V5.12.4, Goddard Earth Sciences Data and Information Services Center  
560 (GES DISC) [data set], <https://doi.org/10.5067/HM00OHQBHKTP>, 2015.

561

562 Rittger, K., Lenard, S. J., Palomaki, R. T., Bair, E. H., Dozier, J. & Mankoff, K. (2025). Historical MODIS/Terra L3 Global  
563 Daily 500m SIN Grid Snow Cover, Snow Albedo, and Snow Surface Properties. (SPIRES\_HIST, Version 1). [Data Set].  
564 Boulder, Colorado USA. National Snow and Ice Data Center. <https://doi.org/10.7265/a3vr-c014>. [describe subset used if  
565 applicable]. Date Accessed 04-27-2026.

566

567 Sengupta, M., Habte, A., Andreas, A., Reda, I., Jaker, S., Xie, Y., Yang, J., Gotseff, P., Kutchenreiter, M., and Shi, Y.: Sky  
568 Radiometers on Stand for Downwelling Radiation (SKYRAD60S), 2021-09-01 to 2023-06-16, ARM Mobile Facility  
569 (GUC), Gunnison, CO; AMF2 (main site for SAIL) (M1), Atmospheric Radiation Measurement (ARM) User Facility [data  
570 set], <https://doi.org/10.5439/1377836>, 2021.

571

572 Vermote, E. F. and Vermeulen, A.: MODIS Algorithm Theoretical Background Document, Atmospheric Correction  
573 Algorithm: Spectral Reflectances (MOD09GA) Version 4.0, NASA, [https://modis.gsfc.nasa.gov/data/atbd/atbd\\_mod08.pdf](https://modis.gsfc.nasa.gov/data/atbd/atbd_mod08.pdf),  
574 last access: 22 October 2022.

575

576 Zhu, Z., Wang, D., Jane, M., Cromwell, E., Sturm, M., Irving, K., and Delamere, J.: Weighing Bucket Precipitation Gauge  
577 (WBPLUVIO2), 2021-09-01 to 2023-06-16, ARM Mobile Facility (GUC), Gunnison, CO; AMF2 (main site for SAIL)  
578 (M1), Atmospheric Radiation Measurement (ARM) User Facility [data set], <https://doi.org/10.5439/1338194>, 2021.

579

<https://doi.org/10.5194/egusphere-2026-2547>

Preprint. Discussion started: 8 May 2026

© Author(s) 2026. CC BY 4.0 License.



580 U.S. Geological Survey: Watershed Boundary Dataset, [https://www.usgs.gov/national-hydrography/watershed-boundary-](https://www.usgs.gov/national-hydrography/watershed-boundary-dataset)  
581 [dataset](#)